NASA Technical Memorandum 110183
U. S. Army Research Laboratory Technical Report 807

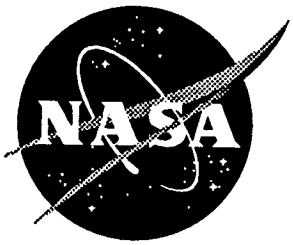

Analytical Investigation of the Hygrothermal Effects and Parametric Study of the Edge Crack Torsion (ECT) Mode III Test Lay-ups

Jian Li
Langley Research Center, Hampton, Virginia

T. Kevin O'Brien
Vehicle Structures Directorate
U.S. Army Research Laboratory
Langley Research Center, Hampton, Virginia

June 1995

National Aeronautics and
Space Administration
Langley Research Center
Hampton, Virginia 23681-0001

ABSTRACT: A shear deformation theory including residual thermal and moisture effects is developed for the analysis of either symmetric or unsymmetric laminates with mid-plane edge delamination under torsion loading. The theory is based on an assumed displacement field which includes shear deformation. The governing equations and boundary conditions are obtained from the principle of virtual work. The analysis of the $[90/(\pm 45)_n/(\mp 45)_n/90]_s$ ECT mode III test lay-up indicates that there are no hygrothermal effects on the mode III strain energy release rate because the laminate, and both sublaminates above and below the delamination, are symmetric lay-ups. A further parametric study reveals that some other lay-ups can have negligible hygrothermal effects even when the sublaminates above and below the delamination are not symmetric about their own mid-planes. However, these lay-ups may suffer from distortion after the curing process. Another interesting set of lay-ups investigated is a class of antisymmetric laminates with $[\pm(\theta/(\theta-90)_2/\theta)]_n$ lay-ups. It is observed that when n takes on even numbers (2 and 4), both hygrothermal and mode I effects can be neglected. From this point of view, these lay-ups provides a way to determine the mode III toughness between two dissimilar layers. However, when n takes on odd numbers (1 and 3), both hygrothermal and mode I effects may be strong in these lay-ups. In particular, when θ equals 45^o, the lay-ups are free from both hygrothermal and mode I effects irrespective of n.

KEY WORDS: laminated composites, fracture toughness, delamination, strain energy release rate, mode III fracture toughness test, torsion.

Nomenclature

a	delamination length, m
A_{ij}	extensional stiffness coefficients, N/m
b	specimen width, m

B_{ij} coupling stiffness coefficients, N

D_{ij} bending and twisting stiffness coefficients, Nm

E_{ii} Young's moduli, GPa

F_X applied tension force, N

g_2 strain energy release rate parameter due to mechanical effect, Nm

g_1 strain energy release rate parameter due to hygrothermal and mechanical coupling effect, N

g_0 strain energy release rate parameter due to hygrothermal effect, N/m

G_T total strain energy release rate, N/m

h half the laminate thickness, m

ΔH percentage moisture weight gain, weight %

I integration constant, m

M_B applied bending moment, Nm

M_T applied twisting moment, Nm

$\{M\}$ vector of stress couples, N

n number of repeats of a group of layers

$\{N\}$ vector of stress resultants, N/m

$\overline{Q}_{ij}$ 3-D transformed reduced stiffness, N/m^2

s characteristic root, 1/m

ΔT temperature change from cure temperature to test temperature, °C

x, y, z Cartesian coordinates

Greek Letters (Symbols)

$\{\alpha\}, \{\overline{\alpha}\}$ lamina coefficients of thermal expansion in lamina and laminate coordinate systems, respectively, per °C

$\{\beta\}, \{\overline{\beta}\}$ lamina coefficients of moisture expansion in lamina and laminate coordinate systems, respectively, per % by weight

ε_0	laminate mid-plane extension strain
ε_{ij}	strain tensor
$\{\varepsilon\}$	vector of in-plane strain components
ϕ_1	extension-twist coupling, m
ϕ_2	bending-twist coupling
$\{\gamma\}$	vector of out-plane shear strain components
η	normalized constant term in M_{xy}, 1/m
$\varphi^1=\varphi^2$	delaminated portion of laminate width, or a, m (see Eq. A-28)
φ^3	undelaminated laminate width, or b-a, m (see Eq. A-28)
λ	laminate torsional stiffness, Nm^2
Λ_1	strain energy parameter due to hygrothermal effect, Nm
Λ_0	strain energy parameter due to hygrothermal effect, N
κ	bending curvature, 1/m
μ_{ij}	shear moduli, GPa
Π	total strain energy per unit laminate length, N
Θ	twisting angle per unit length, or twist, 1/m
Θ^{HT}	twist due to hygrothermal effects, 1/m
θ	fiber angle with respect to x axis for a ply in the laminate
σ_{ij}	stress tensor
$\{\sigma\}$	vector of in-plane stress components
$\{\tau\}$	vector of out-plane shear stress components
$[\Psi_{ij}]$	coefficients that relate the end tension, bending and twisting moments to extension strain, bending curvature and twist Nm^2
$\{\Psi_j\}^{HT}$	force and moments due to hygrothermal effects, Nm^2
Ξ_1, Ξ_2	extension-twist and bending-twist coupling indicators, respectively
Ψ_x, Ψ_y	rotation functions in warping and transverse directions, respectively

Introduction

Delamination is a common failure mode in laminated composites, and often the most serious. Characterization of a laminated composite material for its resistance against such failure has become an important task for damage tolerance design purposes. Delamination in composites is characterized in the fracture mechanics sense by the three modes: mode I (opening), mode II (in-plane shear) and mode III (anti-plane shear). In general, the stress field at the delamination front could be a mixture of all three loading modes. Characterization of fracture resistance, or fracture toughness, in each individual mode for laminated composites can help a designer in materials selection and as a foundation for fracture mechanics criterion used to design against delamination failures.

Analyses and test techniques for mode I delamination fracture toughness have been established [1], and resulted in the publication of an ASTM standard test method D 5528-94a [2]. Mode II fracture toughness characterization [3-7] has also received extensive attention, and standardization development is under way. In the past, the study of mode III fracture toughness had been largely ignored due to the fact that the mode I fracture toughness is much lower than mode III in the traditional laminated composites with epoxy matrices. The lack of a suitable mode III test method at the time was also a factor [8]. As the mode I fracture toughness improves with the development of enhanced resin systems, the two shear failure modes may become more important. Furthermore all the three failure modes are important in the establishment of a mixed mode fracture criterion for structural design purposes.

Recently, an Edge Crack Torsion (ECT) test was proposed as a mode III toughness test method [9]. This test is based on a class of $[90/(\pm 45)_n/(\mp 45)_n/90]_s$ lay-up specimen with a mid-plane free edge delamination subjected to torsion. The ECT test was analyzed based on a shear deformation theory, for its validity as a mode III test [10].

In addition, a simplified solution for the $[90/(\pm 45)_n/(\mp 45)_n/90]_s$ ECT lay-ups was obtained, and a parametric study on the shear modulus effect was also performed [11]. The analytical solution developed in Ref. 10 was restricted to symmetric laminates. Asymmetry in sublaminates (lay-ups above and below the delamination) was considered, but the residual thermal and moisture effects were neglected. The present work is based on the shear deformation theory developed in Ref. 10, but includes the analysis of asymmetrical laminates. The hygrothermal effects are also included. The present solution should be identical to the solution of Ref. 10 on laminate and sublaminate symmetric lay-ups. The present solution will be able to identify the hygrothermal effects neglected in Ref. 10 when the sublaminates are not symmetric. In addition, the present analysis can deal with asymmetric lay-ups as well. In the following, a shear deformation theory including thermal and moisture effects is developed for the analysis of arbitrary composite lay-up with mid-plane edge delamination under torsion loading. The theory is applied to the ECT lay-ups first. Next, a study of some altered ECT lay-ups is presented to assess the thermal and moisture effects on these lay-ups. Finally, the theory is applied to a class of antisymmetric lay-ups.

Mathematical Model

A symmetric or asymmetric laminate with mid-plane free edge delamination is subjected to torsion loading as shown in Fig. 1. The delamination is assumed to run through the entire length of the laminate. The laminate is modeled as three sublaminates as shown in Fig. 2. Sublaminate 1 and 2 represent the portions of the laminate above and below the delamination, while sublaminate 3 represents the undelaminated portion.

Displacement Field

The laminate is assumed to be loaded at its ends in such a way that the stresses do not vary along the x axis. The resultant of the stresses at a typical cross section reduce to

a twisting moment as shown in Fig. 1. If the laminate is loaded by a static equivalent twisting moment at the ends, the stresses do not depend on the x axis at locations away from both ends by virtue of the St.-Venant principle [12]. Such a state of deformation fits the definition of the so called generalized plane deformation [13]. By following the derivation of Ref. 13, the displacement field may be written as

$$\left.\begin{aligned} \mathrm{u}(x,y,z) &= \varepsilon_0 \cdot x + \kappa \cdot x \cdot (z+\bar{z}) + \kappa_1 \cdot x \cdot (y+\bar{y}) + U_0(y,z) \\ \mathrm{v}(x,y,z) &= -\tfrac{1}{2}\kappa_1 \cdot x^2 + \Theta \cdot x \cdot (z+\bar{z}) + V_0(y,z) \\ \mathrm{w}(x,y,z) &= -\tfrac{1}{2}\kappa \cdot x^2 - \Theta \cdot x \cdot (y+\bar{y}) + W_0(y,z) \end{aligned}\right\} \qquad (1)$$

where u, v, and w denote displacements along the x, y, and z axes, respectively. The axial extension is denoted by ε_0, while the bending curvatures in the x-z plane and x-y plane are denoted by κ and κ_1, respectively. The angle of rotation per unit length about the x-axis, or twist, is denoted by Θ.

The constant $\bar{z}$ represents the z-coordinate distance of sublaminate mid-plane with respect to the delamination plane; $\bar{z}$=0 for sublaminate 3 because the sublaminate mid-plane coincide with the delamination plane, $\bar{z}=h/2$ for sublaminate 1, and $\bar{z}=-h/2$ for sublaminate 2. The constant $\bar{y}$ is the distance between the twisting center and the delamination tip and hence is identical for all three sublaminates. The twisting center is initially unknown, and $\bar{y}$ does not show up in the expressions of torsional stiffness and total strain energy release rate of the laminate as will be seen in the final analysis.

The bending curvature κ_1 is neglected because the thickness-to-width ratio of the laminate is much smaller than unity. Further simplification is achieved by considering first order terms only in the Taylor expansion of the displacement functions U_0 and V_0 with respective to the reference surface, and neglecting thickness (z) dependence in function W_0 as the following:

$$\left.\begin{aligned} U_0(y,z) &= U_0(y,0) + \frac{\partial U_0(y,0)}{\partial z}\cdot z + O\left(z^2\right) + \cdots \\ V_0(y,z) &= V_0(y,0) + \frac{\partial V_0(y,0)}{\partial z}\cdot z + O\left(z^2\right) + \cdots \\ W_0(y,z) &= W_0(y,0) + O(z) + \cdots \end{aligned}\right\} \tag{2}$$

Neglecting the terms of $O(z^2)$ and higher for U_0, V_0 and $O(z)$ and higher for W_0 in Equation 2 and substituting the rest into Equation 1 yields

$$\left.\begin{aligned} \mathrm{u}(x,y,z) &= \varepsilon_0 \cdot x + \kappa \cdot x \cdot (z+\bar{z}) + U(y) + z\cdot \psi_x(y) \\ \mathrm{v}(x,y,z) &= \Theta \cdot x \cdot (z+\bar{z}) + V(y) + z\cdot \psi_y(y) \\ \mathrm{w}(x,y,z) &= -\tfrac{1}{2}\kappa \cdot x^2 - \Theta \cdot x \cdot (y+\bar{y}) + W(y) \end{aligned}\right\} \tag{3}$$

Shear deformation is recognized through the rotations ψ_x and ψ_y. Displacement functions U, V, W, ψ_x and ψ_y are functions of y only. These displacement functions will be determined from the governing equations and boundary conditions in section following the next section on constitutive relationships.

The strains corresponding to this displacement field can be written as

$$\{\varepsilon\} = \begin{Bmatrix} \varepsilon_{xx} \\ \varepsilon_{yy} \\ \gamma_{xy} \end{Bmatrix} = \begin{Bmatrix} \varepsilon^o_{xx} \\ \varepsilon^o_{yy} \\ \gamma^o_{xy} \end{Bmatrix} + z\cdot \begin{Bmatrix} \kappa_{xx} \\ \kappa_{yy} \\ \kappa_{xy} \end{Bmatrix} \tag{4}$$

$$\{\gamma\} = \begin{Bmatrix} \gamma_{yz} \\ \gamma_{xz} \end{Bmatrix} = \begin{Bmatrix} \gamma^o_{yz} \\ \gamma^o_{xz} \end{Bmatrix} \tag{5}$$

where

$$\left.\begin{array}{lll} \varepsilon^o_{xx} = \varepsilon_0 + \kappa \cdot \bar{z} & \kappa_{xx} = \kappa & \gamma^o_{yz} = \psi_y + W_{,y} \\ \varepsilon^o_{yy} = V_{,y} & \kappa_{yy} = \psi_{y,y} & \gamma^o_{xz} = \psi_x - \Theta \cdot (y + \bar{y}) \\ \gamma^o_{xy} = U_{,y} + \Theta \cdot \bar{z} & \kappa_{xy} = \psi_{x,y} + \Theta & \end{array}\right\} \tag{6}$$

where partial differentiation by a variable is denoted by the subscript comma followed by that variable.

Constitutive Relationships

A generic sublaminate along with stress resultants and moment couples is shown in Fig. 3. The stress resultants and moment couples are denoted by N_x, N_y, N_{xy}, Q_x, Q_y, M_x, M_y and M_{xy} as shown in Fig. 3. The constitutive relationships can be written in terms of stress resultants and moment couples and associated strains and curvatures as follows

$$\begin{Bmatrix} N_x \\ N_y \\ N_{xy} \\ \hline M_x \\ M_y \\ M_{xy} \end{Bmatrix} = \left[\begin{array}{ccc|ccc} A_{11} & A_{12} & A_{16} & B_{11} & B_{12} & B_{16} \\ A_{12} & A_{22} & A_{26} & B_{12} & B_{22} & B_{26} \\ A_{16} & A_{26} & A_{66} & B_{16} & B_{26} & B_{66} \\ \hline B_{11} & B_{12} & B_{16} & D_{11} & D_{12} & D_{16} \\ B_{12} & B_{22} & B_{26} & D_{12} & D_{22} & D_{26} \\ B_{16} & B_{26} & B_{66} & D_{16} & D_{26} & D_{66} \end{array}\right] \begin{Bmatrix} \varepsilon^o_{xx} \\ \varepsilon^o_{yy} \\ \gamma^o_{xy} \\ \hline \kappa_{xx} \\ \kappa_{yy} \\ \kappa_{xy} \end{Bmatrix} - \begin{Bmatrix} N_x \\ N_y \\ N_{xy} \\ \hline M_x \\ M_y \\ M_{xy} \end{Bmatrix}^{HT} \tag{7}$$

$$\begin{Bmatrix} Q_y \\ Q_x \end{Bmatrix} = \begin{bmatrix} A_{44} & A_{45} \\ A_{45} & A_{55} \end{bmatrix} \begin{Bmatrix} \gamma^o_{yz} \\ \gamma^o_{xz} \end{Bmatrix} \tag{8}$$

where

$$(\{N\},\ \{M\}) = \int_{-h/2}^{h/2} \{\sigma\} \cdot (1,\ z) \cdot dz \tag{9}$$

$$\begin{Bmatrix} Q_y \\ Q_x \end{Bmatrix} = \int_{-h/2}^{h/2} \{\tau\} \cdot dz \tag{10}$$

$$\{\sigma\} = \begin{pmatrix} \sigma_{xx} & \sigma_{yy} & \tau_{xy} \end{pmatrix}^T = \left[\overline{Q}\right] \left\langle \{\varepsilon\} - \{\overline{\alpha}\} \Delta T - \left\{\overline{\beta}\right\} \Delta H \right\rangle \tag{11}$$

$$\{\tau\} = \begin{Bmatrix} \tau_{yz} \\ \tau_{xz} \end{Bmatrix} = \begin{bmatrix} \overline{Q}_{44} & \overline{Q}_{45} \\ \overline{Q}_{45} & \overline{Q}_{55} \end{bmatrix} \{\gamma\} \tag{12}$$

$$\left(A_{ij},\ B_{ij},\ D_{ij}\right) = \int_{-h/2}^{h/2} \overline{Q}_{ij} \cdot \left(1,\ z,\ z^2\right) \cdot dz \tag{13}$$

$$\left(\{N\}^{HT},\ \{M\}^{HT}\right)=\int_{-h/2}^{h/2}\left[\overline{Q}\right]\left\langle\{\overline{\alpha}\}\Delta T+\left\{\overline{\beta}\right\}\Delta H\right\rangle\cdot(1,\ \ z)\cdot dz \tag{14}$$

$\overline{Q}_{ij}$ = the transformed reduced stiffness [14]

$\{\overline{\alpha}\}$= $(\overline{\alpha}_{xx}\ \overline{\alpha}_{yy}\ \overline{\alpha}_{xy})^T$ lamina coefficient of thermal expansion in x-y coordinates

$\{\overline{\beta}\}$= $(\overline{\beta}_{xx}\ \overline{\beta}_{yy}\ \overline{\beta}_{xy})^T$ lamina coefficient of hygroscopic expansion in x-y coordinates

ΔT= temperature differential from cure temperature to test temperature, and

ΔH= percentage moisture weight gain.

For sublaminate 3, the integrations in Equations 9, 10, 13 and 14 should be carried out from $-h$ to h.

Governing Equations

Because all the strains and stresses are independent about the x axis, a unit length of the laminate along the x axis is considered. For all three sublaminates, the upper and lower surfaces are stress free. The governing equations and boundary conditions for the three sublaminates can be obtained from the principle of virtue work:

$$\iint_{\Omega^1}\sigma_{ij}^1\,\delta\varepsilon_{ij}^1\,dydz+\iint_{\Omega^2}\sigma_{ij}^2\,\delta\varepsilon_{ij}^2\,dydz+\iint_{\Omega^3}\sigma_{ij}^3\,\delta\varepsilon_{ij}^3\,dydz=\int_{\Gamma^1+\Gamma^2+\Gamma^3}F_i\,\delta u_i\,ds \tag{15}$$

where Ω^1, Ω^2, Ω^3 represent the volumes of sublaminate 1, 2 and 3, respectively, while Γ^1, Γ^2 and Γ^3 represent their respective boundaries. In order to distinguish similar quantities of the sublaminates, superscripts 1, 2 and 3 are used to refer to the respective sublaminate. In the event of a quantity raised to a power, the quantity will be bracketed.

By following the procedures presented in Ref. 10, the governing equations obtained from Equation 15 for each of the sublaminate may be simplified as

$$N_y^j = N_{xy}^j = M_y^j = Q_y^j = 0, \quad j = 1,2,3 \tag{16}$$

$$M_{xy,y}^j - Q_x^j = 0, \quad j = 1,2,3 \tag{17}$$

The boundary conditions and continuity conditions are

$$M_{xy}^3\Big|_{y=-(b-a)} = 0 \tag{18}$$

$$M_{xy}^1\Big|_{y=a} = M_{xy}^2\Big|_{y=a} = 0 \tag{19}$$

$$M_{xy}^3\Big|_{y=0} = M_{xy}^1\Big|_{y=0} + M_{xy}^2\Big|_{y=0} \tag{20}$$

$$\psi_x^1\Big|_{y=0} = \psi_x^2\Big|_{y=0} = \psi_x^3\Big|_{y=0} \tag{21}$$

Solutions for the Displacement Functions

Substituting the stress resultants and moment couples given in Equations 7 and 8 into Equation 16, and using Equation 6 yields

$$\begin{Bmatrix} V_{,y}^j \\ U_{,y}^j + \Theta \cdot \bar{z}^j \\ \psi_{y,y}^j \end{Bmatrix} = -[R^j]\begin{Bmatrix} \varepsilon_0 \\ \kappa \end{Bmatrix} - \left\{\bar{R}^j\right\} \cdot \left(\psi_{x,y}^j + \Theta\right) + \left\{\hat{R}^j\right\}, \quad j = 1,2,3 \tag{22}$$

$$\psi_y^j + W_{,y}^j = -\frac{A_{45}^j}{A_{44}^j}\left[\psi_x^j - \Theta \cdot (y + \bar{y})\right], \quad j = 1,2,3 \tag{23}$$

where $[R^j]$, $\{\bar{R}^j\}$ and $\{\hat{R}^j\}$ are given in Equations (A-1) through (A-3) of the Appendix.

The remaining non-zero stress resultants and moment couples can be simplified as

$$\begin{Bmatrix} N_x^j \\ M_x^j \\ M_{xy}^j \end{Bmatrix} = \left[\xi^j\right]\begin{Bmatrix} \varepsilon_0 \\ \kappa \end{Bmatrix} + \left\{\bar{\xi}^j\right\}\left(\psi_{x,y}^j + \Theta\right) + \left\{\hat{\xi}^j\right\}, \quad j = 1,2,3 \tag{24}$$

$$Q_x^j = \left[A_{55}^j - \frac{\left(A_{45}^j\right)^2}{A_{44}^j}\right]\left[\psi_x^j - \Theta \cdot (y + \bar{y})\right], \quad j = 1,2,3 \tag{25}$$

The matrix $[\xi^j]$ and vectors $\{\bar{\xi}^j\}$ and$\{\hat{\xi}^j\}$ are given in Equations (A-4) through (A-6) of the Appendix.

The solution of ψ_x for each sublaminate can be obtained by applying Equation 17 to the three regions respectively and making use of the boundary conditions given in Equations 18 through 21. The general form of ψ_x can be written as

$$\psi_x^j = I^j \cdot (e^{s^j \cdot y} + e^{2s^j \cdot \rho^j} \cdot e^{-s^j \cdot y}) + \frac{\eta^j}{s^j} e^{s^j \cdot \rho^j} \cdot e^{-s^j \cdot y} + \Theta \cdot (y + \bar{y}), \quad j = 1,2,3 \tag{26}$$

where I^j represents the integration constant, ρ^j is replaced by -(b-a) for sublaminate 3, and by a for sublaminate 1 and 2, respectively. The integration constant is different from each sublaminate. The three constants for the three sublaminates are given in Equation (A-7) of the Appendix.

The characteristic root s^j and parameter η^j in Equation 26 are given by

$$s^j = \sqrt{\left[A_{55}^j - \frac{\left(A_{45}^j\right)^2}{A_{44}^j} \right] \Big/ \bar{\xi}_3^j}, \quad j = 1,2,3 \tag{27}$$

$$\eta^j = \frac{\xi_{31}^j}{\xi_3^j} \varepsilon_0 + \frac{\xi_{32}^j}{\xi_3^j} \kappa + 2\Theta + \frac{\hat{\xi}_3^j}{\xi_3^j}, \quad j = 1,2,3 \tag{28}$$

Loading Conditions

The extension force, bending and twisting moments for the entire laminate cross-section are denoted by F_X, M_B and M_T, respectively. These are expressed as

$$F_X = \int_{-(b-a)}^{0} N_x^3 \cdot dy + \int_0^a \left(N_x^1 + N_x^2 \right) \cdot dy \tag{29}$$

$$M_B = \int_{-(b-a)}^{0} M_x^3 \cdot dy + \int_0^a \left[M_x^1 + M_x^2 + \bar{z}^1 \cdot N_x^1 + \bar{z}^2 \cdot N_x^2 \right] dy \tag{30}$$

$$M_T = 2\int_{-(b-a)}^{0} M_{xy}^3 \cdot dy + 2\int_0^a \left[M_{xy}^1 + M_{xy}^2 + \bar{z}^1 \cdot N_{xy}^1 + \bar{z}^2 \cdot N_{xy}^2 \right] \cdot dy \tag{31}$$

Substituting the stress resultants and moment couples from Equations 24 for the three sublaminates into Equations 29 through 31 yields

$$\begin{Bmatrix} F_X \\ M_B \\ M_T \end{Bmatrix} = \left[\Psi_{ij}\right] \begin{Bmatrix} \varepsilon_0 \\ \kappa \\ \theta \end{Bmatrix} + \left\{\Psi_j\right\}^{HT} \qquad [i,j = 1,2,3] \tag{32}$$

The parameters Ψ_{ij} in Equation 32 are functions of sublaminate stiffness coefficients (A_{ij}, B_{ij}, D_{ij}) and specimen geometry (a, b, h) and are given in Equation (A-18) of the Appendix. The parameters Ψ_j^{HT} represent the thermal and moisture contributions, and their expressions are given in Equation (A-19) of the Appendix.

The strain ε_0, bending curvature κ and twist Θ can be written as a combination of the mechanical and hygrothermal contributions as

$$\begin{Bmatrix} \varepsilon_0 \\ \kappa \\ \Theta \end{Bmatrix} = \begin{Bmatrix} \varepsilon_0 \\ \kappa \\ \Theta \end{Bmatrix}^M + \begin{Bmatrix} \varepsilon_0 \\ \kappa \\ \Theta \end{Bmatrix}^{HT} \tag{33}$$

where

$$\begin{Bmatrix} \varepsilon_0 \\ \kappa \\ \Theta \end{Bmatrix}^{HT} = -\left[\Psi_{ij}\right]^{-1} \left\{\Psi_j\right\}^{HT} \tag{34}$$

For a laminate under torsion loading, F_X=M_B=0, the induced extension strain and bending curvature can be written as

$$\varepsilon_0 = \phi_1 \cdot \Theta + \phi_1^{HT} \tag{35}$$

$$\kappa = \phi_2 \cdot \Theta + \phi_2^{HT} \tag{36}$$

where

$$\begin{Bmatrix}\phi_1\\ \phi_2\end{Bmatrix} = -\begin{bmatrix}\Psi_{11} & \Psi_{12}\\ \Psi_{21} & \Psi_{22}\end{bmatrix}^{-1}\begin{Bmatrix}\Psi_{13}\\ \Psi_{23}\end{Bmatrix} \tag{37}$$

$$\begin{Bmatrix}\phi_1\\ \phi_2\end{Bmatrix}^{HT} = -\begin{bmatrix}\Psi_{11} & \Psi_{12}\\ \Psi_{21} & \Psi_{22}\end{bmatrix}^{-1}\begin{Bmatrix}\Psi_1\\ \Psi_2\end{Bmatrix}^{HT} \tag{38}$$

Parameters ϕ_1 and ϕ_2 represent extension-twist and bending-twist couplings, respectively.

The twisting moment can be obtained from Equation 32 as

$$M_T = \lambda \cdot \left(\Theta - \Theta^{HT}\right) \tag{39}$$

where

$$\lambda = \phi_1 \cdot \Omega_{31} + \phi_2 \cdot \Omega_{32} + \Omega_{33} \tag{40}$$

The coefficient λ represents the laminate torsional stiffness.

Strain Energy and Strain Energy Release Rate

The strain energy per unit length of the laminate can be written as

$$\Pi = \frac{1}{2}\sum_{j=1}^{3}\left(\int_{\Omega^j}\left\langle\{\varepsilon\} - \{\overline{\alpha}\}\cdot\Delta T - \{\overline{\beta}\}\cdot\Delta H\right\rangle^T\{\sigma\}\cdot dy\cdot dz + \int_{\Omega^j}\{\gamma\}^T\{\tau\}\,dy\cdot dz\right) \tag{41}$$

Substituting Equation 11 into Equation 41, rearranging yields

$$\Pi = \frac{1}{2}\sum_{j=1}^{3}\int_{\Omega^j}\left(\{\varepsilon\}^T\{\sigma\} + \{\gamma\}^T\{\tau\}\right)\cdot dy\cdot dz - \frac{1}{2}\sum_{j=1}^{3}\int_{\Omega^j}\left\langle\{\overline{\alpha}\}\cdot\Delta T + \{\overline{\beta}\}\cdot\Delta H\right\rangle^T[\overline{Q}]\{\varepsilon\}\cdot dy\cdot dz$$
$$+\frac{1}{2}\sum_{j=1}^{3}\int_{\Omega^j}\left\langle\{\overline{\alpha}\}\cdot\Delta T + \{\overline{\beta}\}\cdot\Delta H\right\rangle^T[\overline{Q}]\left\langle\{\overline{\alpha}\}\cdot\Delta T + \{\overline{\beta}\}\cdot\Delta H\right\rangle\cdot dy\cdot dz \tag{42}$$

The last term in Equation 42 does not depend on delamination length a, hence will not

be considered further. The first term in Equation 42, Π_1, could be easily proved to be

$$\Pi_1 = \frac{1}{2} \cdot \left(\varepsilon_0 \cdot F_X + \kappa \cdot M_B + \Theta \cdot M_T \right) \tag{43}$$

For a laminate under torsion loading, Equation 43 reduces to

$$\Pi_1 = \frac{1}{2} \cdot \Theta \cdot M_T = \frac{1}{2} \cdot \lambda \cdot \Theta \cdot \left(\Theta - \Theta^{HT} \right) \tag{44}$$

The second term in Equation 42, Π_2, may be written as

$$\Pi_2 = -\frac{1}{2} \Theta \cdot \Lambda_1 - \frac{1}{2} \Lambda_0 \tag{45}$$

Parameters Λ_1 and Λ_0 are functions of delamination length, a, and given in Equations (A-26) and (A-27) of the Appendix.

For the laminate (as show in Fig. 1) containing a planar delamination of length a that extends under a constant twist Θ, no external work is performed as the delamination extends, the total strain energy release rate may be calculated from

$$G_T = -\frac{\partial \Pi}{\partial a} \tag{46}$$

Substituting Equation 44 and 45 into Equation 46 and differentiating yields

$$G_T = -\frac{1}{2} \lambda_{,a} \cdot \Theta^2 + \frac{1}{2} \left(\lambda_{,a} \cdot \Theta^{HT} + \lambda \cdot \Theta^{HT}_{,a} + \Lambda_{1,a} \right) \cdot \Theta + \frac{1}{2} \Lambda_{0,a} \tag{47}$$

In order to isolate the hygrothermal effects, the total strain energy release rate can be written in terms of mechanical twist by substituting Equation 33 into 47 to yield

$$G_T = \frac{1}{2} g_2 \cdot \left(\Theta^M \right)^2 + \frac{1}{2} g_1 \cdot \Theta^M + \frac{1}{2} g_0 \tag{48}$$

where

$$g_2 = -\lambda_{,a} \tag{49}$$

$$g_1 = \lambda \cdot \Theta^{HT}_{,a} - \lambda_{,a} \cdot \Theta^{HT} + \Lambda_{1,a} \tag{50}$$

$$g_0 = \lambda \cdot \Theta^{HT}_{,a} \cdot \Theta^{HT} + \Lambda_{0,a} \tag{51}$$

Parameter g_2 represents the mechanical contribution to the strain energy release rate, while parameter g_1 is the coefficient of the cross term representing the coupling of hygrothermal and mechanical contributions, and g_0 represents the hygrothermal contribution. Equation 47 indicates that there could be a non zero strain energy release rate due to hygrothermal effects alone.

Mode III Lay-up Identification

The presence of extension-twist and bending-twist couplings in a laminate with arbitrary lay-up may induce mode I and mode II contributions to the total stain energy release rate in addition to the mode III contribution. The objective here is to identify the mode I and II contribution to the total strain energy release rate in order to minimize them. The actual evaluation of mode I and II components is not necessary. Instead, the closed form solution given in Equation 36 may provide a convenient alternative to identify the presence of mode I and II contributions. Substituting Equation 40 into Equation 49 yields

$$g_2 = -\Psi_{33,a} - \left(\phi_{1,a}\Psi_{31} + \phi_1\Psi_{31,a}\right) - \left(\phi_{2,a}\Psi_{32} + \phi_2\Psi_{32,a}\right) \tag{52}$$

The second and third terms in Equation 52 indicate the presence of mode I and II contributions due to extension-twist and bending-twist couplings, respectively. Both these terms should be zero for pure mode III lay-ups. If for a particular lay-up these two terms are very small compared to the first term, this lay-up may be considered as a

desirable mode III lay-up. The $[90/(\pm 45)_n/(\mp 45)_n/90]_s$ ECT lay-ups belong to this category. Two indicators are defined to help the identification of desirable mode III lay-ups as follows

$$\Xi_1 = \frac{\left(\phi_{1,a}\Psi_{31} + \phi_1\Psi_{31,a}\right)}{\Psi_{33,a} + \left(\phi_{1,a}\Psi_{31} + \phi_1\Psi_{31,a}\right) + \left(\phi_{2,a}\Psi_{32} + \phi_2\Psi_{32,a}\right)} \tag{53}$$

$$\Xi_2 = \frac{\left(\phi_{2,a}\Psi_{32} + \phi_2\Psi_{32,a}\right)}{\Psi_{33,a} + \left(\phi_{1,a}\Psi_{31} + \phi_1\Psi_{31,a}\right) + \left(\phi_{2,a}\Psi_{32} + \phi_2\Psi_{32,a}\right)} \tag{54}$$

where Ξ_1 and Ξ_2 are extension-twist and bending-twist coupling indicators, respectively. Note that these indicators are percentages of the second and third terms to the total term in Equation 52.

Results

First, the present analytical solution was compared with Ref. 10 and 11 for the ECT lay-ups $[90/(\pm 45)_n/(\mp 45)_n/90]_s$. The lamina properties are given in Table 1. The hygrothermal bending curvature and twist defined in Equation 33 vanish for these ECT lay-ups because of the laminate and sublaminate symmetry. For these ECT lay-ups, the present solution should be identical to that of Ref. 10. Tables 2 and 3 show the comparisons of torsional stiffness and strain energy release rate parameter (g_2) predicted by the present solution and Ref. 10 and 11. The present solution is identical to Ref. 10 as seen in Tables 2 and 3. Also observed is the accuracy of the simplified solution given in Ref. 11 for the ECT lay-ups.

Altered ECT Lay-ups

Second, the present analytical solution was used to investigate the residual thermal effect for several lay-ups selected by altering the $[90/(\pm 45)_3/(\mp 45)_3/90]_s$ ECT lay-up and are presented in Table 4. The lamina properties from Table 1 were used to

generate the analytical solutions and are presented in Table 5 for a delamination length a/b=0.3. The temperature change ΔT=-156°C was used. The moisture weight gain ΔH was assumed to be zero to isolate the residual thermal effects.

All these altered lay-ups have higher torsional stiffness (λ) than the original ECT lay-up when one compares the stiffness values in Table 5 to the corresponding value in Table 2. The thermal-mechanical coupling strain energy release rate parameter (g_1) is zero, and the thermal parameter (g_0) is negligible compared to the magnitude (~1000 N/m) of the mode III toughness obtained from experiments [9]. The small amount of g_0 is due to the asymmetry in the sublaminates. The symmetry of the entire laminate however results in the coupling parameter g_1 to diminish. The extension-twist coupling indicator (Ξ_1) vanishes for all the lay-ups because there is no extension-twist coupling in these lay ups.

The bending-twist coupling indicator (Ξ_2) is very small for these lay-ups as shown in Table 5 (0.6%<). Both lay-ups L1 and L2 have six pairs of ±45° layers in each sublaminate, the bending-twist coupling indicator of L1 is one order of magnitude smaller than that of L2 due to self-symmetry arrangemet of the ±45° layers in L1. The bending-twist coupling indicator is higher in lay-up L3 than that in lay-up L4 where the out-most 90° layer from the ECT lay-up has been changed to 45° and -45°, respectively. There are three and two pairs of ±45° layers in each sublaminate of lay-up L5 and L6, respectively. The bending-twist coupling indicator is higher in lay-up L6 than that in lay-up L5, but still less than 0.6%. All these lay-ups may be considered as desirable mode III lay-ups from the dominance of mode III strain energy release rate point of view. However, these lay-ups may suffer from distortion after curing process due to asymmetry in the sublaminates.

Antisymmetric Lay-ups

The lay-ups studied above are all symmetric laminates and show little thermal effect on the strain energy release rate. The analytical model developed in Section 2 is not limited to symmetric laminates. Next, a class of asymmetric laminates are considered to investigate the residual thermal and moisture effects. These lay-ups are a class of antisymmetric laminates with $[\pm(\theta/(\theta-90)_2/\theta)]_n$ lay-ups. The sublaminates may be either symmetric (n=odd number) or antisymmetric (n=even number). This class of laminates exhibits extension-twist coupling, and does not distort after curing.

Results for lay-ups $\theta=30^o$ and n=1 to 4 are presented in Table 6 for a normalized delamination length a/b=0.3. The moisture weight gain, ΔH, was assumed to be zero when the results in Table 6 were generated. Both torsional stiffness, strain energy release rate parameters and extension-twist coupling indicator are presented in the table. The bending-twist coupling indicator vanishes because there is no bending-twist coupling. The thermal parameter g_0 is zero for all the lay-ups due to the symmetry or antisymmetry of the sublaminates. The presence of the coupling parameter g_1 and the extension-twist coupling indicator are strong when the sublaminates are symmetric (n=1 and 3). However, the significance of parameter g_1 and mode I indicator reduces as n increases. The moisture effect may also be strong in these lay-ups. Fig. 4 shows the moisture effects on the coupling parameter g_1 as a function of delamination length a/b for n=3 with a fixed temperature change of ΔT=-156 °C. As the percentage moisture weight gain ΔH increases from zero, parameter g_1 reduces and becomes zero (canceling the thermal effect) when ΔH=0.0208 irrespective of the delamination length. Further increase of ΔH changes the sign of g_1.

When the sublaminates are antisymmetric (n=2 and 4), both the thermal-mechanical coupling parameter g_1 and the extension-twist coupling indicator are very

small. From this point of view, these lay-ups could be candidate mode III lay-ups to characterize the mode III fracture toughness between two layers with different fiber orientations. Additional results for $\theta=20^o$, 40^o, 45^o, 50^o, 60^o and 70^o when n=4 are presented in Table 7 along with $\theta=30^o$. The torsional stiffness λ, strain energy release rate parameter g_2 and the extension-twist coupling indicator are symmetric with respective to $\theta=45^o$ as seen from Table 7. Both parameter g_1 and the extension-twist coupling indicator are very small and become identical zero when $\theta=45^o$.

The torsional stiffness (λ) and strain energy release rate parameter (g_2) as a function of normalized delamination length (*a/b*) are plotted in Fig. 5 and 6 for $\theta=30^o$, 45^o. The torsional stiffness decreases as the delamination length increases, and reaches the torsional stiffness of the two sublaminates as the delamination completely separates the laminate in to two pieces. The middle portion of the curve is almost linear. The curve becomes flat near both ends (*a/b*=0 and 1). This indicates that both very small and very large delamination lengths are not desirable for mode III delamination growth because the available strain energy release rate to drive the delamination is proportional to the derivative of the torsional stiffness. Fig. 6 is essentially the negative value of the derivative of the torsional stiffness. It is seen from Fig. 4 through 6 that the analytical solution gives meaningful results for the entire range of normalized delamination length (a/b=0 to 1).

Concluding Remarks

A shear deformation theory including hygrothermal effects is developed for the analysis of either symmetric or asymmetric laminates with mid-plane edge delamination under torsion loading. The torsional stiffness and total strain energy release rate are obtained in closed form. The hygrothermal effects on the strain energy release rate are identified by hygrothermal-mechanical coupling and pure hygrothermal contributions.

Two indicators are defined to identify the presence of mode I and mode II contributions in the total strain energy release rate.

The analysis of the $[90/(\pm 45)_n/(\mp 45)_n/90]_s$ ECT mode III lay-ups indicates that there are no hygrothermal effects on the strain energy release rate because of the laminate and sublaminate symmetry. Identical results to those obtained in Ref. 10 are observed for these ECT lay-ups. A further study of some altered ECT lay-ups reveals that these lay-ups have negligible residual thermal and bending-twist coupling effects even when the sublaminates above and below the delamination are not symmetric about their own mid-planes. However, these lay-ups may suffer from distortion after the curing process.

Another set of lay-ups investigated is a class of antisymmetric laminates with $[\pm(\theta/(\theta-90)_2/\theta)]_n$ lay-ups There is no bending-twist coupling effect in these lay-ups. When n takes on odd numbers (1 and 3), both the thermal and extension-twist coupling effects on the total strain energy release rate may be strong. The relative significance of the thermal and extension-twist coupling effects reduces as n increases. The moisture effect may also be strong in these lay-ups. However, the moisture effect tends to reduce the thermal effect, and may cancel the thermal effect at some value of the percentage moisture weight gain irrespective of the delamination length.

When n takes on even numbers (2 and 4), both the hygrothermal and extension-twist coupling effects may be neglected. From this point of view, these lay-ups are desirable mode III lay-ups to characterize the mode III fracture toughness between two $\pm\theta$ layers. In particular, when $\theta=45^o$, both the hygrothermal and extension-twist coupling effects vanish irrespective of n.

Acknowledgment This work was performed while the first author was a National Research Council Research Associate at NASA Langley Research Center.

References

[1] O'Brien, T. K. and Martin, R. H., "Round Robin Testing for Mode I Interlaminar Fracture Toughness of Composite Materials," *Journal of Composites Technology and Research*, Vol. 15, No. 4, Winter 1993, pp. 269-281.

[2] D 5528-94a, Standard Test Method for Mode I Interlaminar Fracture Toughness of Unidirectional Fiber-Reinforced Polymer Matrix Composites, 1994 *Annual Book of ASTM Standards*, Vol. 15.03, pp. 272-281.

[3] Russell, A. J., "On the Measurement of Mode II Interlaminar Energies," DREP Materials Report 82-0, Defense Research Establishment Pacific, Victoria, BC, 1982.

[4] Salpekar, S. A., Raju, I. S. and O'Brien, T. K., "Strain Energy Release Rate Analysis of the End-Notched Flexure Specimen Using the Finite Element Method," *Journal of Composites Technology and Research*, Vol. 10, No. 4, Winter 1988, pp. 133-139.

[5] O'Brien, T. K., Murri, G. B. and Salpekar, S. A., "Interlaminar Shear Fracture Toughness and Fatigue Thresholds for Composite Materials," *Composite Materials: Fatigue and Fracture, Second Volume, ASTM STP 1012*, April, 1989, pp. 222-250.

[6] Carlsson, L. A. and Gillespie, J. W., "Mode-II Interlaminar Fracture of Composites," in *Application of Fracture Mechanics to Composite Materials*, Composite Materials Series, 6, Klaus Friedrich, Ed., Elsevier, 1989, pp. 113-157.

[7] Tanaka, K., Kageyama, K. and Hojo, M., "Prestandardization Study on Mode II Interlaminar Fracture Toughness Test for CFRP in Japan," *Composites*, Vol. 26, No. 4, 1995, pp. 257-267.

[8] Martin, R. H., "Evaluation of the Split Cantilever Beam for Mode III Delamination Testing," *Composite Materials: Fatigue and Fracture, Third Volume, ASTM STP 1110*, T. K. O'Brien, Ed., American Society for Testing and Materials, Philadelphia,

1991, pp. 243-266.

[9] Lee, S. M., "An Edge Crack Torsion Method for Mode III Delamination Fracture Testing," *Composite Technology & Research*, Vol. 15, No. 3, Fall 1993, pp. 193-201.

[10] Li, J. and Wang, Y., "Analysis of a Symmetric Laminate with Mid-Plane Free Edge Delamination Under Torsion: Theory and Application to the Edge Crack Torsion (ECT) Specimen for Mode III Toughness Characterization," *Engineering Fracture Mechanics*, Vol. 49, No. 2, 1994, pp. 179-194.

[11] Li, J. and O'Brien, T. K., "Simplified Data Reduction Methods for the ECT Test for Mode III Interlaminar Fracture Toughness," *Journal of Composites Technology and Research*, submitted 1995, (also available as NASA TM 110176, May 1995).

[12] Love, A. E. H., *A Treatise of the Mathematical Theory of Elasticity,* 4th Edition, Dover Publication, 1944, p. 173, pp. 19-21.

[13] Lekhnitskii, S. G., *Theory of Elasticity of an Anisotropic Body*, Holden-Day, Inc., San Francisco,1963, pp. 103-108.

[14] Vinson, J. R. and Sierakowski, R. L., *The Behavior of Structures Composed of Composite Materials*, Martinus Nijhoff Publishers, 1986, pp. 46-47.

[15] Daniel, I. M. and Ishai, O., *Engineering Mechanics of Composite Materials,* Oxford University Press, Inc., 1994, p. 35.

Appendix : Definition of Parameters

In this appendix, all the intermediate parameters needed to evaluate the torsional stiffness and strain energy release rate are summarized according to their sequence of appearance in the text.

The matrix $[R^j]$ and vectors $\{\overline{R}^j\}$ and $\{\hat{R}^j\}$ in Equation 22 are given by

$$\left[R^{j}\right]=\begin{bmatrix} A_{22}^{j} & A_{26}^{j} & B_{22}^{j} \\ A_{26}^{j} & A_{66}^{j} & B_{26}^{j} \\ B_{22}^{j} & B_{26}^{j} & D_{22}^{j} \end{bmatrix}^{-1}\begin{bmatrix} A_{12}^{j} & A_{12}^{j}\cdot\bar{z}^{j}+B_{12}^{j} \\ A_{16}^{j} & A_{16}^{j}\cdot\bar{z}^{j}+B_{16}^{j} \\ B_{12}^{j} & B_{12}^{j}\cdot\bar{z}^{j}+D_{12}^{j} \end{bmatrix},\quad j=1,2,3 \tag{A-1}$$

$$\left[\bar{R}^{j}\right]=\begin{bmatrix} A_{22}^{j} & A_{26}^{j} & B_{22}^{j} \\ A_{26}^{j} & A_{66}^{j} & B_{26}^{j} \\ B_{22}^{j} & B_{26}^{j} & D_{22}^{j} \end{bmatrix}^{-1}\begin{Bmatrix} B_{26}^{j} \\ B_{66}^{j} \\ D_{26}^{j} \end{Bmatrix},\quad j=1,2,3 \tag{A-2}$$

$$\left[\hat{R}^{j}\right]=\begin{bmatrix} A_{22}^{j} & A_{26}^{j} & B_{22}^{j} \\ A_{26}^{j} & A_{66}^{j} & B_{26}^{j} \\ B_{22}^{j} & B_{26}^{j} & D_{22}^{j} \end{bmatrix}^{-1}\begin{Bmatrix} N_{y}^{j} \\ N_{xy}^{j} \\ M_{y}^{j} \end{Bmatrix}^{HT},\quad j=1,2,3 \tag{A-3}$$

where $\bar{z}^{1}=-\bar{z}^{2}=h/2$, and $\bar{z}^{3}=0$.

The matrix $[\xi^{j}]$ and vectors $\{\bar{\xi}^{j}\}$ and $\{\hat{\xi}^{j}\}$ in Equation 24 are given by

$$\left[\xi^{j}\right]=\begin{bmatrix} A_{11}^{j} & A_{11}^{j}\cdot\bar{z}^{j}+B_{11}^{j} \\ B_{11}^{j} & B_{11}^{j}\cdot\bar{z}^{j}+D_{11}^{j} \\ B_{16}^{j} & B_{16}^{j}\cdot\bar{z}^{j}+D_{16}^{j} \end{bmatrix}-\begin{bmatrix} A_{12}^{j} & A_{16}^{j} & B_{12}^{j} \\ B_{12}^{j} & B_{16}^{j} & D_{12}^{j} \\ B_{26}^{j} & B_{66}^{j} & D_{26}^{j} \end{bmatrix}\left[R^{j}\right],\quad j=1,2,3 \tag{A-4}$$

$$\left[\bar{\xi}^{j}\right]=\begin{Bmatrix} B_{16}^{j} \\ D_{16}^{j} \\ D_{66}^{j} \end{Bmatrix}-\begin{bmatrix} A_{12}^{j} & A_{16}^{j} & B_{12}^{j} \\ B_{12}^{j} & B_{16}^{j} & D_{12}^{j} \\ B_{26}^{j} & B_{66}^{j} & D_{26}^{j} \end{bmatrix}\left[\bar{R}^{j}\right],\quad j=1,2,3 \tag{A-5}$$

$$\left[\hat{\xi}^{j}\right]=\begin{bmatrix} A_{12}^{j} & A_{16}^{j} & B_{12}^{j} \\ B_{12}^{j} & B_{16}^{j} & D_{12}^{j} \\ B_{26}^{j} & B_{66}^{j} & D_{26}^{j} \end{bmatrix}\left[\hat{R}^{j}\right]-\begin{Bmatrix} N_{x}^{j} \\ M_{x}^{j} \\ M_{xy}^{j} \end{Bmatrix}^{HT}, \tag{A-6}$$

The integration constant, I^{j}, in Equation 26 is given by

$$I^{j}=I_{jk}\eta^{k},\quad j,k=1,2,3 \tag{A-7}$$

The explicit expressions of I_{jk} are given in the following

$$\Delta\cdot I_{11}=\bar{\xi}_{3}^{1}\left\{1-\left[1+\frac{\bar{\xi}_{3}^{3}}{\bar{\xi}_{3}^{1}}\frac{s^{3}}{s^{1}}th(s^{3}\cdot(b-a))+\frac{\bar{\xi}_{3}^{2}}{\bar{\xi}_{3}^{1}}\frac{s^{2}}{s^{1}}th(s^{2}\cdot a)\right]e^{s^{1}\cdot a}\right\} \tag{A-8}$$

$$\Delta \cdot I_{12} = \bar{\xi}_3^2 \left\{ 1 - \left[1 - th(s^2 \cdot a) \right] e^{s^2 \cdot a} \right\} \tag{A-9}$$

$$\Delta \cdot I_{13} = -\bar{\xi}_3^3 \left\{ 1 - \left[1 + th(s^3 \cdot (b-a)) \right] e^{-s^3 \cdot (b-a)} \right\} \tag{A-10}$$

$$\left[1 + e^{2s^2 \cdot a} \right] \cdot I_{21} = I_{11} \cdot \left(1 + e^{2s^1 \cdot a} \right) + \frac{1}{s^1} e^{s^1 \cdot a} \tag{A-11}$$

$$\left[1 + e^{2s^2 \cdot a} \right] \cdot I_{22} = I_{12} \cdot \left(1 + e^{2s^1 \cdot a} \right) - \frac{1}{s^2} e^{s^2 \cdot a} \tag{A-12}$$

$$\left[1 + e^{2s^2 \cdot a} \right] \cdot I_{23} = I_{13} \cdot \left(1 + e^{2s^1 \cdot a} \right) \tag{A-13}$$

$$\left[1 + e^{-2s^3 \cdot (b-a)} \right] \cdot I_{31} = I_{11} \cdot \left(1 + e^{2s^1 \cdot a} \right) + \frac{1}{s^1} e^{s^1 \cdot a} \tag{A-14}$$

$$\left[1 + e^{-2s^3 \cdot (b-a)} \right] \cdot I_{32} = -I_{12} \cdot \left(1 + e^{2s^1 \cdot a} \right) \tag{A-15}$$

$$\left[1 + e^{-2s^3 \cdot (b-a)} \right] \cdot I_{33} = I_{13} \cdot \left(1 + e^{2s^1 \cdot a} \right) - \frac{1}{s^3} e^{-s^3 \cdot (b-a)} \tag{A-16}$$

where

$$\Delta = \left(1 + e^{2s^1 \cdot a} \right) \left[s^3 \cdot \bar{\xi}_3^3 \cdot th(s^3 \cdot (b-a)) + s^1 \cdot \bar{\xi}_3^1 \cdot th(s^1 \cdot a) + s^2 \cdot \bar{\xi}_3^2 \cdot th(s^2 \cdot a) \right] \tag{A-17}$$

The matrix $[\Psi_{ij}]$ and vector $\{\Psi_j^{HT}\}$ in Equation 32 are given by

$$\left[\Psi_{ij} \right] = \begin{bmatrix} \xi_{11}^1 + \xi_{11}^2 & \xi_{12}^1 + \xi_{12}^2 & 2\bar{\xi}_1^1 + 2\bar{\xi}_1^2 \\ \xi_{21}^1 + \xi_{21}^2 + \frac{h}{2}\left(\xi_{11}^1 - \xi_{11}^2 \right) & \xi_{22}^1 + \xi_{22}^2 + \frac{h}{2}\left(\xi_{12}^1 - \xi_{12}^2 \right) & 2\left[\bar{\xi}_2^1 + \bar{\xi}_2^2 + \frac{h}{2}\left(\bar{\xi}_1^1 - \bar{\xi}_1^2 \right) \right] \\ 2\xi_{31}^1 + 2\xi_{31}^2 & 2\xi_{32}^1 + 2\xi_{32}^2 & 4\bar{\xi}_3^1 + 4\bar{\xi}_3^2 \end{bmatrix} \cdot a$$
$$+ \begin{bmatrix} \xi_{11}^3 & \xi_{12}^3 & 2\bar{\xi}_1^3 \\ \xi_{21}^3 & \xi_{22}^3 & 2\bar{\xi}_2^3 \\ 2\xi_{31}^3 & 2\xi_{32}^3 & 4\bar{\xi}_3^3 \end{bmatrix} \cdot (b-a) + \begin{bmatrix} \bar{\xi}_1^1 & \bar{\xi}_1^2 & \bar{\xi}_1^3 \\ \bar{\xi}_2^1 + \frac{h}{2}\bar{\xi}_1^1 & \bar{\xi}_2^2 - \frac{h}{2}\bar{\xi}_1^2 & \bar{\xi}_2^3 \\ 2\bar{\xi}_3^1 & 2\bar{\xi}_3^2 & 2\bar{\xi}_3^3 \end{bmatrix} \begin{bmatrix} f_1^1 & f_2^1 & 2f_3^1 \\ f_1^2 & f_2^2 & 2f_3^2 \\ f_1^3 & f_2^3 & 2f_3^3 \end{bmatrix} \tag{A-18}$$

$$\left\{ \Psi_j^{HT} \right\} = \begin{Bmatrix} \hat{\xi}_1^1 + \hat{\xi}_1^2 \\ \hat{\xi}_2^1 + \hat{\xi}_2^2 + \frac{h}{2}\left(\hat{\xi}_1^1 - \hat{\xi}_1^2 \right) \\ \xi_3^1 + \xi_3^2 \end{Bmatrix} a + \begin{Bmatrix} \hat{\xi}_1^3 \\ \hat{\xi}_2^3 \\ \xi_3^3 \end{Bmatrix} (b-a) + \begin{bmatrix} \bar{\xi}_1^1 & \bar{\xi}_1^2 & \bar{\xi}_1^3 \\ \bar{\xi}_2^1 + \frac{h}{2}\bar{\xi}_1^1 & \bar{\xi}_2^2 - \frac{h}{2}\bar{\xi}_1^2 & \bar{\xi}_2^3 \\ \bar{\xi}_3^1 & \bar{\xi}_3^2 & \bar{\xi}_3^3 \end{bmatrix} \begin{Bmatrix} f_1^{HT} \\ f_2^{HT} \\ f_3^{HT} \end{Bmatrix} \tag{A-19}$$

where

$$f_i^j = -\left(\frac{\xi_{3i}^1}{\xi_3^1} I_{j1} + \frac{\xi_{3i}^2}{\xi_3^2} I_{j2} + \frac{\xi_{3i}^3}{\xi_3^3} I_{j3}\right)\left(e^{s^j \cdot a} - 1\right)^2 - \frac{1}{s^j}\frac{\xi_{3i}^j}{\xi_3^j}\left(e^{s^j \cdot a} - 1\right), \; i = 1,2 \;\; j = 1,2 \qquad \text{(A-20)}$$

$$f_i^j = \left(\frac{\xi_{3i}^1}{\xi_3^1} I_{j1} + \frac{\xi_{3i}^2}{\xi_3^2} I_{j2} + \frac{\xi_{3i}^3}{\xi_3^3} I_{j3}\right)\left(e^{-s^j \cdot (b-a)} - 1\right)^2 + \frac{1}{s^j}\frac{\xi_{3i}^j}{\xi_3^j}\left(e^{-s^j \cdot (b-a)} - 1\right), \; i = 1,2 \; j = 3 \qquad \text{(A-21)}$$

$$f_3^j = -\left(I_{j1} + I_{j2} + I_{j3}\right)\left(e^{s^j \cdot a} - 1\right)^2 - \frac{1}{s^j}\left(e^{s^j \cdot a} - 1\right), \; j = 1,2 \qquad \text{(A-22)}$$

$$f_3^j = \left(I_{j1} + I_{j2} + I_{j3}\right)\left(e^{-s^j \cdot (b-a)} - 1\right)^2 + \frac{1}{s^j}\left(e^{-s^j \cdot (b-a)} - 1\right), \quad j = 3 \qquad \text{(A-23)}$$

$$f_j^{HT} = -\left(\frac{\hat{\xi}_3^1}{\xi_3^1} I_{j1} + \frac{\hat{\xi}_3^2}{\xi_3^2} I_{j2} + \frac{\hat{\xi}_3^3}{\xi_3^3} I_{j3}\right)\left(e^{s^j \cdot a} - 1\right)^2 - \frac{1}{s^j}\frac{\hat{\xi}_3^j}{\xi_3^j}\left(e^{s^j \cdot a} - 1\right), \quad j = 1,2 \qquad \text{(A-24)}$$

$$f_j^{HT} = \left(\frac{\hat{\xi}_3^1}{\xi_3^1} I_{j1} + \frac{\hat{\xi}_3^2}{\xi_3^2} I_{j2} + \frac{\hat{\xi}_3^3}{\xi_3^3} I_{j3}\right)\left(e^{-s^j \cdot (b-a)} - 1\right)^2 + \frac{1}{s^j}\frac{\hat{\xi}_3^3}{\xi_3^3}\left(e^{-s^j \cdot (b-a)} - 1\right), \quad j = 3 \qquad \text{(A-25)}$$

The parameters Λ_1 and vector Λ_0 in Equation 45 are given by

$$\begin{aligned}
\Lambda_1 = {} & \phi_1 \left\{ b\left(N_x^3\right)^{HT} - \sum_{j=1}^{3}\left[\left(N_y^j\right)^{HT} R_{11}^j + \left(N_{xy}^j\right)^{HT} R_{21}^j + \left(M_y^j\right)^{HT} R_{31}^j\right]\varphi^j \right\} \\
& + \phi_2 \left\{ b\left(M_x^3\right)^{HT} - \sum_{j=1}^{3}\left[\left(N_y^j\right)^{HT} R_{12}^j + \left(N_{xy}^j\right)^{HT} R_{22}^j + \left(M_y^j\right)^{HT} R_{32}^j\right]\varphi^j \right\} \\
& + \sum_{j=1}^{3}\left[\left(M_{xy}^j\right)^{HT} - \left(N_y^j\right)^{HT} \overline{R}_1^j - \left(N_{xy}^j\right)^{HT} \overline{R}_2^j - \left(M_y^j\right)^{HT} \overline{R}_3^j\right]\overline{\psi}^j
\end{aligned} \qquad \text{(A-26)}$$

$$\begin{aligned}
\Lambda_0 = {} & \phi_1^{HT} \left\{ b\left(N_x^3\right)^{HT} - \sum_{j=1}^{3}\left[\left(N_y^j\right)^{HT} R_{11}^j + \left(N_{xy}^j\right)^{HT} R_{21}^j + \left(M_y^j\right)^{HT} R_{31}^j\right]\varphi^j \right\} \\
& + \phi_2^{HT} \left\{ b\left(M_x^3\right)^{HT} - \sum_{j=1}^{3}\left[\left(N_y^j\right)^{HT} R_{12}^j + \left(N_{xy}^j\right)^{HT} R_{22}^j + \left(M_y^j\right)^{HT} R_{32}^j\right]\varphi^j \right\} \\
& + \sum_{j=1}^{3}\left[\left(M_{xy}^j\right)^{HT} - \left(N_y^j\right)^{HT} \overline{R}_1^j - \left(N_{xy}^j\right)^{HT} \overline{R}_2^j - \left(M_y^j\right)^{HT} \overline{R}_3^j\right]\overline{\psi}^j \\
& + \sum_{j=1}^{3}\left[\left(N_y^j\right)^{HT} \hat{R}_1^j + \left(N_{xy}^j\right)^{HT} \hat{R}_2^j + \left(M_y^j\right)^{HT} \hat{R}_3^j\right]\varphi^j
\end{aligned} \qquad \text{(A-27)}$$

where

$$\varphi^1 = \varphi^2 = a \quad \varphi^3 = b - a \tag{A-28}$$

$$\overline{\psi}^{\mathrm{j}} = -I_{\mathrm{jk}} \cdot \overline{\eta}^{\mathrm{k}} \cdot \left(e^{s^{\mathrm{j}} \cdot a} - 1\right)^2 - \frac{\overline{\eta}^{\mathrm{j}}}{s^{\mathrm{j}}}\left(e^{s^{\mathrm{j}} \cdot a} - 1\right) + 2a, \mathrm{j} = 1,2 \quad \mathrm{k} = 1,2,3 \tag{A-29}$$

$$\overline{\psi}^{\mathrm{j}} = I_{\mathrm{jk}} \cdot \overline{\eta}^{\mathrm{k}} \cdot \left(e^{-s^{\mathrm{j}} \cdot (b-a)} - 1\right)^2 + \frac{\overline{\eta}^{\mathrm{j}}}{s^{\mathrm{j}}}\left(e^{-s^{\mathrm{j}} \cdot (b-a)} - 1\right) + 2(b-a), \ \mathrm{j} = 3 \quad \mathrm{k} = 1,2,3 \tag{A-30}$$

$$\hat{\psi}^{\mathrm{j}} = -I_{\mathrm{jk}} \hat{\eta}^{\mathrm{k}} \left(e^{s^{\mathrm{j}} \cdot a} - 1\right)^2 - \frac{\hat{\eta}^{\mathrm{j}}}{s^{\mathrm{j}}}\left(e^{s^{\mathrm{j}} \cdot a} - 1\right), \mathrm{j} = 1,2 \quad \mathrm{k} = 1,2,3 \tag{A-31}$$

$$\hat{\psi}^{\mathrm{j}} = I_{\mathrm{jk}} \cdot \hat{\eta}^{\mathrm{k}} \cdot \left(e^{-s^{\mathrm{j}} \cdot (b-a)} - 1\right)^2 + \frac{\hat{\eta}^{\mathrm{j}}}{s^{\mathrm{j}}}\left(e^{-s^{\mathrm{j}} \cdot (b-a)} - 1\right), \ \mathrm{j} = 3 \quad \mathrm{k} = 1,2,3 \tag{A-32}$$

$$\overline{\eta}^{\mathrm{k}} = \frac{\xi_{31}^{\mathrm{k}}}{\xi_3^{\mathrm{k}}}\phi_1 + \frac{\xi_{32}^{\mathrm{k}}}{\xi_3^{\mathrm{k}}}\phi_2 + 2, \qquad \mathrm{k} = 1,2,3 \tag{A-33}$$

$$\hat{\eta}^{\mathrm{k}} = \frac{\xi_{31}^{\mathrm{k}}}{\xi_3^{\mathrm{k}}}\phi_1^{\mathrm{HT}} + \frac{\xi_{32}^{\mathrm{k}}}{\xi_3^{\mathrm{k}}}\phi_2^{\mathrm{HT}} + \frac{\hat{\xi}_3^{\mathrm{k}}}{\xi_3^{\mathrm{k}}}, \qquad \mathrm{k} = 1,2,3 \tag{A-34}$$

TABLE 1-- Elastic properties and configurational parameters of Carbon/Epoxy composite [9]

Properties*		Configurational Parameters
E_{11}=165 GPa	α_1=-0.3 × 10^{-6} /°C	b=38.1 mm (Width)
E_{22}=E_{33}=10.3 GPa	α_2=30 × 10^{-6} /°C	t=0.13 mm (Ply thickness)
μ_{12}=μ_{13}=5.5 GPa	β_1=0	h=Half laminate thickness
μ_{23}=5.5 GPa	β_2=0.2	
ν_{12}=ν_{13}=0.28	ΔT=-156 °C	
ν_{23}=0.28		

* These thermal and moisture expansion coefficients are adopted from a similar carbon/epoxy (IM6/SC1081) material [15] because such information was not available in Ref. 9.

TABLE 2-- Comparison of torsional stiffness and strain energy release rate parameter g_2 for the ECT lay-up $[90/(\pm 45)_n/(\mp 45)_n/90]_s$ with n=3

n=3	λ (Nm²)			g_2 (Nm)		
a/b	Present	Ref. 10	Ref. 11	Present	Ref. 10	Ref. 11
0.1	17.49	17.49	17.53	426.4	426.4	424.4
0.3	14.06	14.06	14.11	451.0	451.1	449.7
0.5	10.60	10.60	10.66	450.1	450.2	448.8
0.7	7.244	7.244	7.311	434.6	434.7	433.3
0.9	4.434	4.434	4.510	223.7	223.9	223.1

TABLE 3-- Comparison of torsional stiffness strain energy release rate parameter g_2 for the ECT lay-up $[90/(\pm 45)_n/(\mp 45)_n/90]_s$ with n=4

n=4	λ (Nm²)			g_2 (Nm)		
a/b	Present	Ref. 10	Ref. 11	Present	Ref. 10	Ref. 11
0.1	37.19	37.19	37.24	859.7	859.8	855.9
0.3	29.82	29.82	29.88	985.9	986.0	985.7
0.5	22.27	22.27	22.36	976.5	976.6	976.3
0.7	15.13	15.13	15.23	890.7	890.8	890.5
0.9	9.852	9.852	9.964	360.0	360.2	359.6

TABLE 4-- Altered ECT lay-ups and their representative codes.

Code	Lay-up
L1	$[(\pm 45)_3/(\mp 45)_3/0/90]_s$
L2	$[(\pm 45)_6/\ 0/90]_s$
L3	$[45/(\pm 45)_3/(\mp 45)_3/90]_s$
L4	$[-45/(\pm 45)_3/(\mp 45)_3/90]_s$
L5	$[(\pm 45_2)_3/0/90]_s$
L6	$[(\pm 45_3)_2/0/90]_s$

TABLE 5-- Torsional stiffness, total energy release rate parameters and bending-twist coupling indicator for the altered ECT lay-ups at a/b=0.3

Code	λ (Nm^2)	g_2 (Nm)	g_1 (N)	g_0 (N/m)	Ξ_2 %
L1	16.39	567.4	0	0.040	-0.002
L2	16.31	561.7	0	0.040	-0.057
L3	16.06	526.5	0	0.278	-0.323
L4	16.54	531.0	0	0.277	-0.185
L5	15.91	549.5	0	0.040	-0.234
L6	15.24	529.2	0	0.041	-0.544

TABLE 6-- Torsional stiffness, total energy release rate parameters, and extension-twist coupling indicator for $[\pm(30/-60_2/30)]_n$ lay-ups at a/b=0.3

n	λ (Nm^2)	g_2 (Nm)	g_1 (N)	g_0 (N/m)	Ξ_1 %
1*	.247	5.244	8.078	0	-64.5
3	8.49	247.7	33.05	0	4.1
2**	2.39	74.98	-0.5×10^{-5}	0	0.3×10^{-5}
4	19.5	599.4	-0.042	0	0.003

*$[(30/-60_2/30)\underset{\uparrow}{/}(-30/60_2/-30)]$

**$[(30/-60_2/30/-30/60_2/-30)\underset{\uparrow}{/}(30/60_2/30/-30/60_2/-30)]$

Note that $\uparrow$ indicates the interface with free edge delamination.

TABLE 7-- Torsional stiffness, total energy release rate parameters, and extension-twist coupling indicator for $[\pm(\theta/(90\text{-}\theta)_2/\theta)]_4$ lay-ups at a/b=0.3

θ	λ (Nm^2)	g_2 (Nm)	g_1 (N)	Ξ_1 %
20	12.6	347.9	-0.004	0.0003
30	19.5	599.4	-0.042	0.003
40	24.3	745.1	-0.046	0.002
45	25.0	765.0	0	0
50	24.3	745.1	0.046	0.002
60	19.5	599.4	0.042	0.003
70	12.6	374.9	0.004	0.0003

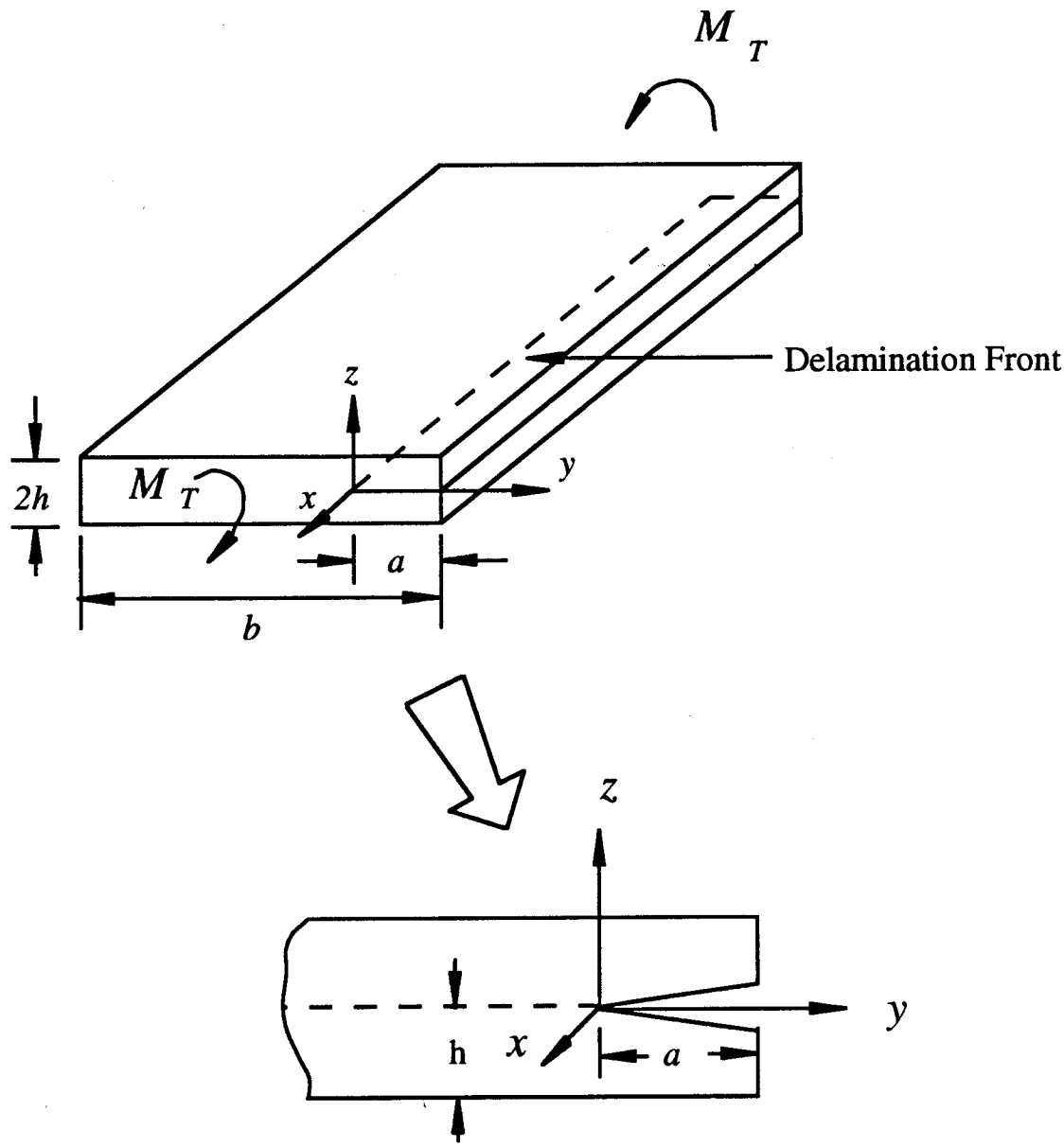

FIG. 1-- A laminate with mid-plane edge delamination under torsion loading.

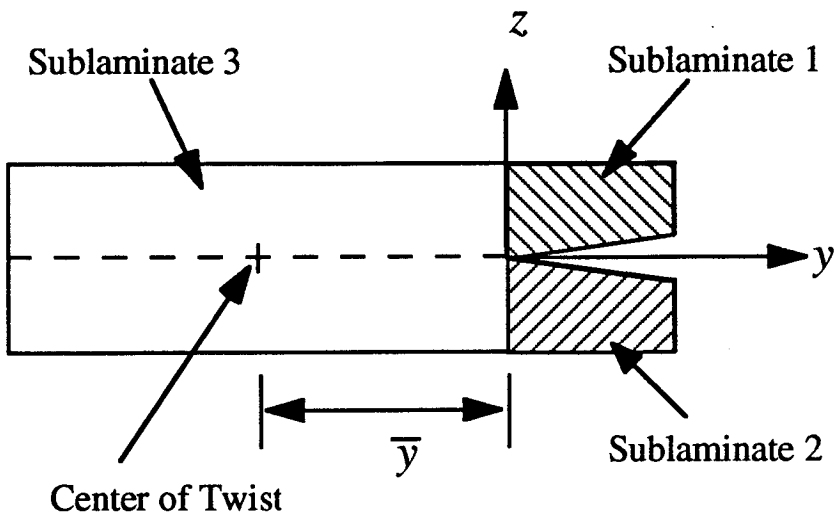

FIG. 2-- A typical x= constant plane of the delaminated laminate.

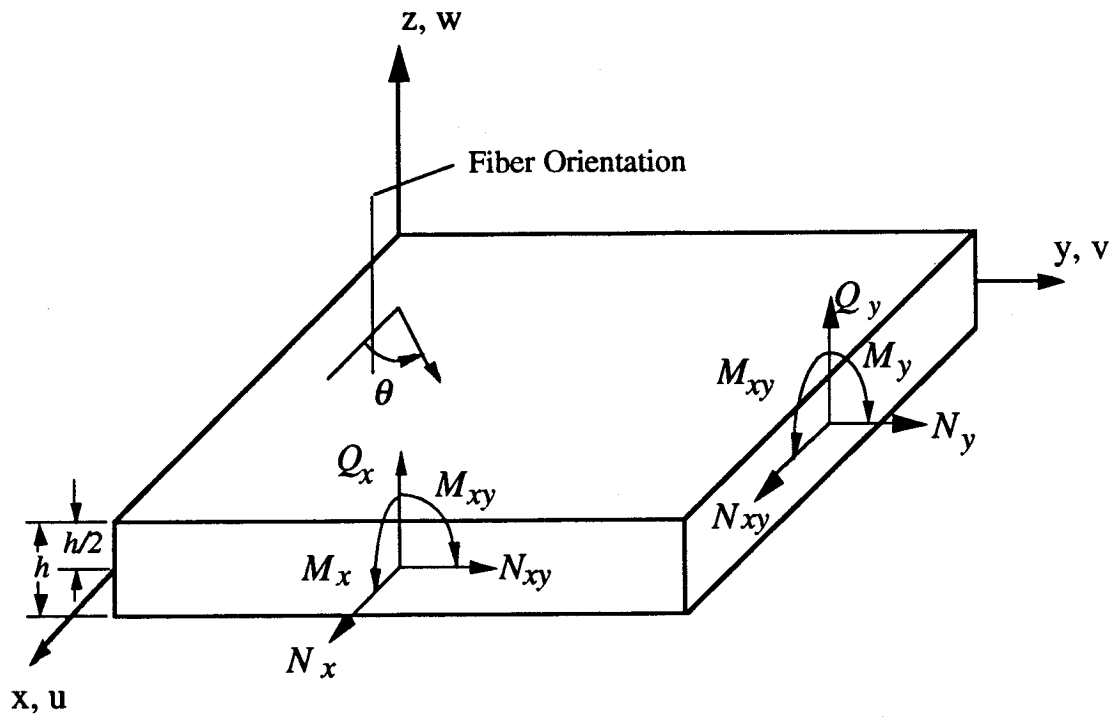

FIG. 3-- Notation and sign convention for stress resultants and moment couples.

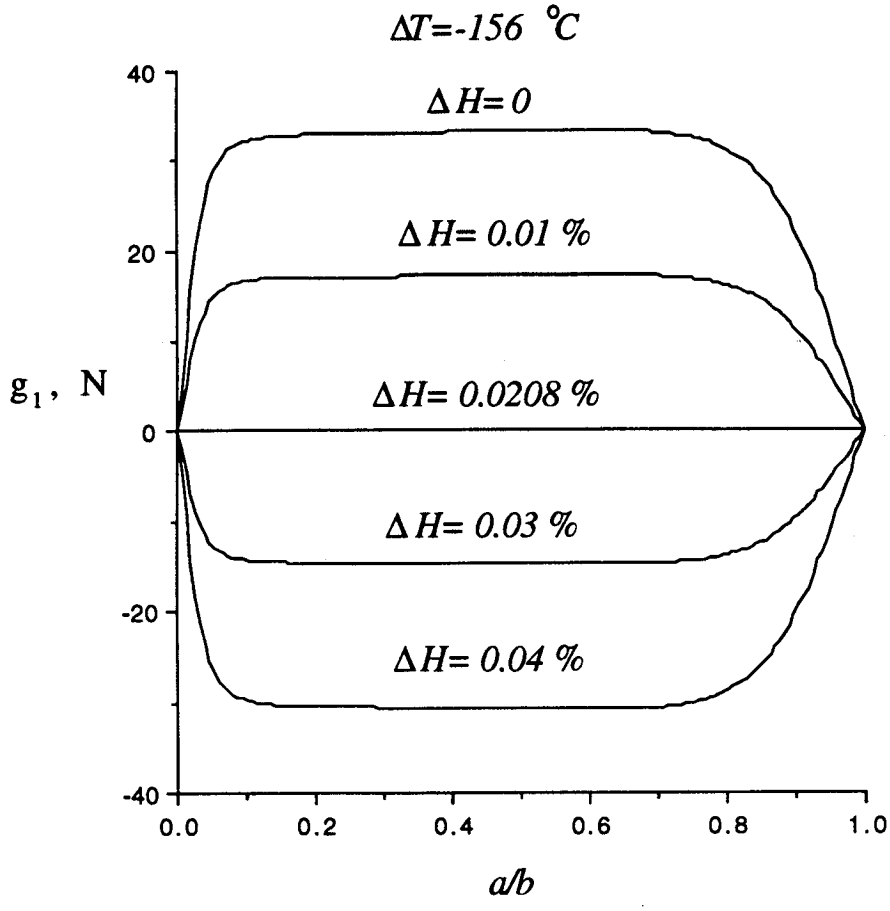

FIG. 4-- Coupling strain energy release rate parameter, g_1, as a function of normalized delamination length, *a/b*, for $[\pm(30/-60_2/30]_3$ lay-up.

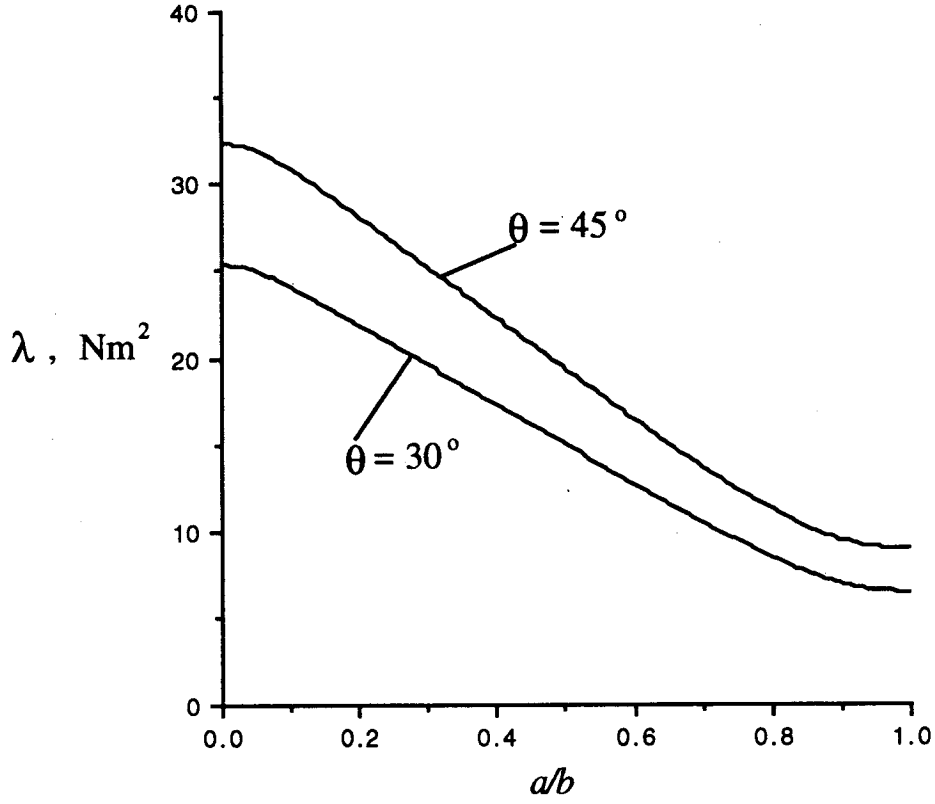

FIG. 5-- Torsional stiffness, λ, as a function of normalized delamination length, *a/b*, for $[\pm(\theta/(90-\theta)_2/\theta]_4$ lay-ups (θ=30°, 45°).

REPORT DOCUMENTATION PAGE

Form Approved
OMB No. 0704-0188

1. AGENCY USE ONLY (Leave blank)	2. REPORT DATE	3. REPORT TYPE AND DATES COVERED
	June 1995	Technical Memorandum

4. TITLE AND SUBTITLE

Analytical Investigation of the Hygrothermal Effects and Parametric Study of the Edge Crack Torsion (ECT) Mode III Test Lay-ups

5. FUNDING NUMBERS

WU 505-63-50-04

6. AUTHOR(S)

Jian Li and T. Kevin O'Brien

7. PERFORMING ORGANIZATION NAME(S) AND ADDRESS(ES)

NASA Langley Research Center
Hampton, VA 23681-0001
Vehicle Structures Directorate, U.S. Army Research Laboratory
NASA Langley Research Center
Hampton, VA 23681-0001

8. PERFORMING ORGANIZATION REPORT NUMBER

9. SPONSORING/MONITORING AGENCY NAME(S) AND ADDRESS(ES)

National Aeronautics and Space Administration
Washington, DC 20546-0001
and
U.S. Army Research Laboratory
Adelphi, MD 20783-1145

10. SPONSORING/MONITORING AGENCY REPORT NUMBER

NASA TM-110183
ARL-TR-807

11. SUPPLEMENTARY NOTES

Li: National Research Council Resident Research Associate, Langley Research Center, Hampton, VA
O'Brien: Vehicle Structures Directorate, ARL, Langley Research Center, Hampton, VA

12a. DISTRIBUTION/AVAILABILITY STATEMENT

Unclassified - Unlimited

Subject Category 24

12b. DISTRIBUTION CODE

13. ABSTRACT *(Maximum 200 words)*

A shear deformation theory including residual thermal and moisture effects is developed for the analysis of either symmetric or unsymmetric laminates with mid-plane edge delamination under torsion loading. The theory is based on an assumed displacement field which includes shear deformation. The governing equations and boundary conditions are obtained from the principle of virtual work. The analysis of the $[90/(\pm 45)_n/(\mp 45)_n/90]_s$ ECT mode III test lay-up indicates that there are no hygrothermal effects on the mode III strain energy release rate because the laminate, and both sublaminates above and below the delamination, are symmetric lay-ups. A further parametric study reveals that some other lay-ups can have negligible hygrothermal effects even when the sublaminates above and below the delamination are not symmetric about their own mid-planes. However, these lay-ups may suffer from distortion after the curing process. Another interesting set of lay-ups investigated is a class of antisymmetric laminates with $[\pm(\theta/(\theta\text{-}90)_2/\theta)]_n$ lay-ups. It is observed that when n takes on even numbers (2 and 4), both hygrothermal and mode I effects can be neglected. From this point of view, these lay-ups provides a way to determine the mode III toughness between two dissimilar layers. However, when n takes on odd numbers (1 and 3), both hygrothermal and mode I effects may be strong in these lay-ups. In particular, when θ equals 45°, the lay-ups are free from both hygrothermal and mode I effects irrespective of n.

14. SUBJECT TERMS

Laminated composites; Fracture toughness; Delamination; Strain energy release rate; Mode III fracture toughness test; Torsion

15. NUMBER OF PAGES

37

16. PRICE CODE

A03

17. SECURITY CLASSIFICATION OF REPORT	18. SECURITY CLASSIFICATION OF THIS PAGE	19. SECURITY CLASSIFICATION OF ABSTRACT	20. LIMITATION OF ABSTRACT
Unclassified	Unclassified		